NASA Technical Memorandum 84898

STRAIN GAGE LOAD MEASUREMENT ON THE SHUTTLE ORBITER

Alan L. Carter

November 1982

NASA

NASA Technical Memorandum 84898

STRAIN GAGE LOAD MEASUREMENT ON THE SHUTTLE ORBITER

Alan L. Carter
Ames Research Center
Dryden Flight Research Facility
Edwards, California

National Aeronautics and Space Administration

1982

STRAIN GAGE LOAD MEASUREMENT ON THE SHUTTLE ORBITER

Alan L. Carter
Chief, Structures Section
NASA Ames Research Center
Dryden Flight Research Facility
Edwards, California

Abstract:

This paper describes the application of the calibrated strain gage load measurement method to the shuttle orbiter. Descriptions of instrumentation and calibration are included, along with comparisons of measured results with wind tunnel and FLEXSTAB analytical predictions.

Symbols:

C_{V_0}	load coefficient at $\alpha = 0°$
C_{V_α}	load coefficient per degree α
$C_{V_{\delta_e}}$	load coefficient per degree δ_e
E_1	thermal slope correction factor
E_2	thermal bias correction factor
F	thermal gradient ratio
M	Mach number
n_z	load factor, g
$\bar{q}$	dynamic pressure, lb/ft^2
R_t	strain reading at time t, $\mu in/in$
R_0	strain reading at reference time, $\mu in/in$
V	shear load, lb
x_0	orbiter fuselage station, in
α	angle of attack, deg
δ_e	elevator position, deg
ε	strain, $\mu in/in$
ε_n	net strain, $\mu in/in$
ε_{n_t}	net strain at time t, $\mu in/in$

Subscripts:

CD	at cool down
WS	at wheel stop

Introduction:

As with conventional aircraft, space transportation reentry vehicle development depends heavily on experimental load verification to expand the operating envelope and to assess useful life. For a number of years, the structures research section at the NASA Ames Research Center, Dryden Flight Research Facility, has been applying the calibrated strain gage load measurement technique to high-speed vehicles, where aerodynamic heating is significant. The basic measurement technique [1] has become the standard approach for experimental verification of design loads for both military and civil aircraft prototypes.

Unfortunately, the thermal gradients produced by aerodynamic heating cause thermal stresses that interfere with strain gage load measurement, as evidenced during the X-15 program. Therefore, a structural heating laboratory was constructed at Dryden to develop techniques for separating mechanical and thermal strain gage outputs. References 2 to 4 discuss tests performed in the laboratory on X-15 components to investigate thermal effects on strain gage load measurement.

A comprehensive program was conducted using the YF-12 aircraft, which was instrumented for strain and temperature, calibrated for load measurement, and flown to Mach 3 speeds, where significant aerodynamic heating was experienced. The vehicle was then returned to the laboratory and heated to simulate the flight environment, and the resulting thermal strain outputs were recorded. These outputs were used to correct the flight strains, to obtain

measured loads. In conjunction with this, thermal, structural, and airloads analyses were performed for comparison with the measured results. Descriptions of the various test and analysis efforts and comparisons are given in Reference 5.

Because of the YF-12 experience, the Dryden structures section was asked to act as a consulting team for the verification of design loads on the shuttle orbiter. The initial orbiter effort was to instrument and calibrate orbiter vehicle 101 (OV 101), which was launched from the back of the B-747 carrier aircraft. Reference 6 describes that program and presents comparisons of measured and predicted loads. This paper describes the vehicle and its instrumentation, explains load measurement procedures, and presents comparisons of measured data with predictions for the orbital flight test (OFT) program.

Vehicle Description:

The orbiter configuration (Fig. 1) is a deep boxy fuselage supported on a double delta wing. Elevons are used for pitch and roll control. Split rudders are used for yaw control and also act as speedbrakes. A body flap is used for additional pitch trim.

The structure is aluminum and is protected against aerodynamic heating by a layer of insulating ceramic tiles. The wing structure (Fig. 2) consists of a main box and a glove separated by a wheel well. The main box is composed of 6 spanwise spars with corrugated webs and 12 chordwise ribs with truss webs. The main covers are aluminum skin-stringer aft of the wheel well (fuselage station (FS) 1191 to 1365), and honeycomb sandwich adjacent to the wheel well (FS 1040 to 1191). The glove is composed of truss stub-spars covered with aluminum skin.

Instrumentation:

Strain gages were installed at three stations on the right wing (Fig. 3). At each station axial gages were installed on the spar caps, and three leg rosettes were installed on the spar webs and on the upper and lower covers between spars (Fig. 4).

In addition, the basic parameters such as airspeed, altitude, angles of attack and sideslip, dynamic pressure, attitude, rates, accelerations, surface control positions, and hinge moments were recorded in flight. Temperature measurements at selected locations on the surface and on the internal structure were also recorded.

The data were recorded on pulse code modulation (PCM) onboard recorders and telemetered to ground stations.

Strain Gage Calibration:

To calibrate the strain gages, the instrumented flight vehicle was supported at the external tank attach points, so that the support reactions acted on the fuselage structure rather than on the wing. Loads were applied with hydraulic actuators, monitored by load cells, acting on wooden load pads in compression, against the lower surface of the wing. The load point locations are shown in Figure 5. Each point was loaded individually, except for a check load condition which loaded three points simultaneously. The strain gages were recorded on a very sensitive laboratory data system, in 20-percent increments of increasing and decreasing load.

Load equations relating shear, bending, and torque loads at each station to strain gage outputs were derived using the multilinear regression technique of Reference 1. Redundant gages were eliminated using the procedure of Reference 7. Sample results are shown in Table 1. The check load condition was not used in the derivation of the load equations. The strains from the check load condition were substituted into the load equations and compared to the applied values. The results are listed in Table 2.

Data Analysis:

The flight recorder tapes were processed at the NASA Johnson Space Center to produce computer compatible tapes (CCTs) in engineering units. Computer programs were written, and Dryden engineers and technicians read the CCTs and processed the data to obtain tabulations and plots of measured loads. The gross flight strains were processed using the relation

$$\varepsilon_{n_t} = E_1\left(R_t - R_0\right) + E_2 \qquad (1)$$

where ε_{n_t} is the net strain at time t, R_t is the reading at time t, R_0 is the reading at zero reference, E_1 is the factor for polarity correction, and E_2 is the factor for thermal correction.

This relation provided corrections for zero, for polarity, and for thermal effects, as discussed in the next section. To establish R_0 values, a flight time was selected, and a special computer program read the CCTs and punched a reference deck containing the appropriate zero values. A time just prior to engine start was used as a reference. The reference deck also contained values of E_1 and E_2 which were set to ±1.0 and 0, respectively, for ascent cases, where there are no significant thermal effects.

Finally, the ε_n values were substituted into the load equations, and the results were printed and plotted along with the basic parameters mentioned in the Instrumentation section.

Thermal Correction:

The investigation described in the Introduction section suggests several possible approaches to correcting for thermal stress effects: (a) the analytical approach, where the structural temperatures, corresponding thermal stresses, and strain gage outputs are determined from theoretical predictions; (b) the experimental approach, where the strain gage outputs are determined through a thermal calibration of the instrumented vehicle; and (c) some combination of the previous approaches.

In the laboratory, it is technically feasible to heat the orbiter (with the tiles removed) to bondline temperatures (that is, the temperatures reached in flight at the interface of the tiles and the aluminum substructure). However, it has not been feasible to fit such a thermal calibration into the program schedule. Experience with the YF-12 aircraft indicated that a very detailed definition of the structural temperature distribution is necessary to predict thermal stresses with sufficient accuracy to provide thermal corrections for load measurement. Unfortunately, there are insufficient in-flight thermal measurements to provide this detailed definition for the orbiter.

Therefore, it was decided to proceed as follows:

(a) Set up detailed heat transfer models of the orbiter structure, predict the structural temperatures for each flight, and compare the predictions with available flight measurements. These models and some sample results are presented in Reference 8.

(b) Set up detailed structural models of the instrumented cross sections to compute thermal stresses. Compare computed data with available test data. This is discussed later in this section.

(c) Install infrared scanners in the shuttle orbiter wing to obtain thermal maps of the structural temperatures in flight. This experiment is in the planning stage.

(d) Generate empirical corrections from postflight readings. To accomplish this, strain gage data are recorded periodically from wheel stop until the vehicle has cooled to soak room temperature, as determined from the temperature measurements. The differences between readings at wheel stop and room temperature are taken to be the result of thermal strains at wheel stop, and therefore will serve as the desired thermal corrections at wheel stop. However, the thermal corrections at earlier times in the descent will be different, depending on the relative thermal gradients between the time of interest and wheel stop. To account for this, analytically predicted and measured temperatures are used to establish the thermal gradient ratio, F, between the time of interest and wheel stop. A plot of F as a function of time is shown in Figure 6.

A special computer program reads the strains for wheel stop (WS) and cool down (CD) from the CCTs, computes the E_2 values from

$$E_2 = \left(\varepsilon_{WS} - \varepsilon_{CD}\right) F$$

and punches a revised reference deck containing R_0, E_1, and E_2 values for each flight. These values are used to compute the net strain, ε_n, for descent cases (Eq. (1)).

To examine the purely analytical approach, predicted and experimentally adjusted temperatures at wheel stop (Fig. 7) were entered into thermal stress analysis models to predict thermal strain gage outputs. These predicted outputs are compared to measured values in Figure 8. Although there is fair correlation, the accuracy is not yet considered good enough for thermal correction of load measurement. Improvements in analytical prediction methods are being developed.

Predicted Loads:

Predicted loads were obtained from theoretical solutions and from wind tunnel data. Theoretical values were generated using the FLEXSTAB computer program [9], which uses the Woodward linear, potential flow, constant pressure panel approach. The aerodynamic model is shown in Figure 9. Cases at specified angle of attack and elevon position were run for a range of Mach numbers from 3.0 to 0.6. The pressures from these computer runs were integrated to the load measurement stations to obtain coefficients C_{V_0}, C_{V_α}, and $C_{V_{\delta_e}}$. These coefficients are used to express the loads as functions of $\bar{q}$, α, and δ_e in the relation

$$V = \bar{q}\left(C_{V_0} + C_{V_\alpha}\,\alpha + C_{V_{\delta_e}}\,\delta_e\right)$$

The stability derivatives produced by the FLEXSTAB analysis were used in a standard five-degree-of-freedom trim analysis program to predict α and δ_e for given values of M, $\bar{q}$, and n_z. With these α and δ_e values, the loads were computed for various flight cases.

The wind tunnel pressure data were also integrated to the load measurement stations to obtain similar solutions as functions of α and δ_e. The loads were then computed using measured α and δ_e values as input.

Comparison of Measured and Predicted Loads:

The postflight correction procedures described in the Thermal Correction section were applied to several flight maneuvers from the second flight of the space transportation system (STS-2). The data presented in this paper are for the wing root station. Figures 10 and 11 show shear, bending, and torque loads as functions of load factor for the Mach 0.8 and Mach 2.1 cases, respectively. Both thermally uncorrected and corrected flight data are compared with FLEXSTAB- and wind-tunnel-predicted values. For the Mach 0.8 case, the corrected flight-measured data agree quite well with both theoretical and wind tunnel predictions. The thermal corrections are significant. The greatest thermal correction was for bending, which is consistent with the observation that the largest thermal stresses are axial stresses in the spar caps and lower cover panels.

For the supersonic case, corrected flight-measured shear and bending loads agree quite well with the FLEXSTAB predictions. The FLEXSTAB and wind tunnel values agree for bending and torque, but the wind tunnel values are about 15 percent higher than the FLEXSTAB values for shear. The largest discrepancy is between measured and predicted torque, although both predicted and measured values are relatively small. This discrepancy indicates that the measured center of pressure is aft of predictions, which is consistent with other data on the orbiter supersonic trim.

Concluding Remarks:

As with conventional aircraft, space transportation reentry vehicle development depends heavily on experimental load verification to expand the operating envelope and to assess useful life. For many years, the Dryden Flight Research Facility has performed load investigations on vehicles such as the X-15 and YF-12 aircraft and now on the shuttle orbiter. The orbiter experience to date indicates that:

(a) The calibrated strain gage load measurement technique, using an empirical thermal correction procedure, is giving reasonable results, based on comparisons with available predictions.

(b) The thermal effects are significant.

The development of analytical thermal correction methodology will require considerable effort. The orbiter program can contribute significantly toward this goal.

References:

1. Skopinski, T. H.; Aiken, William S., Jr.; and Huston, Wilber B.: Calibration of Strain-Gage Installations in Aircraft Structures for the Measurement of Flight Loads. NACA Rept. 1178, 1954.

2. Fields, Roger A.: A Study of the Accuracy of a Flight-Heating Simulation and Its Effect on Load Measurement. NASA TN D-5741, 1970.

3. Fields, Roger A.; Olinger, Frank V.; and Monaghan, Richard C.: Experimental Investigation of Mach 3 Cruise Heating Simulations on a Representative Wing Structure for Flight-Loads Measurement. NASA TN D-6749, 1972.

4. Monaghan, Richard C.; and Fields, Roger A.: Experiments To Study Strain-Gage Load Calibrations on a Wing Structure at Elevated Temperatures. NASA TN D-7390, 1973.

5. NASA YF-12 Flight Loads Program. NASA TM X-3061, 1974.

6. Carter, Alan L.; and Sims, Robert L.: Comparison of Theoretical Predictions of Orbiter Airloads With Wind Tunnel and Flight Test Results for a Mach Number of 0.52. NASA TM-81358, 1981.

7. Tang, Ming H.; and Sheldon, Robert G.: A Modified T-Value Method for Selection of Strain Gages for Measuring Loads on a Low Aspect Ratio Wing. NASA TP-1748, 1980.

8. Ko, William L.; Quinn, Robert D.; Gong, Leslie; Schuster, Lawrence S.; and Gonzales, David: Preflight Reentry Heat Transfer Analysis of Space Shuttle. AIAA Paper 81-2382, 1981.

9. Tinoco, E.; and Mercer, J.: FLEXSTAB—A Summary of the Functions and Capabilities of the NASA Flexible Airplane Analysis Computer System. NASA CR-2564, 1974.

TABLE 1.—WING STATION 134 EQUATIONS

(ε9441 denotes strain from gage 9441)

Shear = 19.315(ε9441) + 2.470(ε9447) - 39.015(ε9666) - 43.947(ε9453)
-145.163(ε9426) - 55.640(ε9679) + 36.772(ε9681) + 36.047(ε9437)

Bending = -1292.484(ε9441) - 896.941(ε9447) + 884.426(ε9666) - 1304.763(ε9453)
-2367.296(ε9426) - 9031.836(ε9679) - 7772.491(ε9681) + 5535.649(ε9437)

Torque = 6458.629(ε9441) + 4512.486(ε9447) - 1735.158(ε9666) + 3062.796(ε9453)
-46436.846(ε9426) - 12773.063(ε9679) + 3644.844(ε9691) + 8938.303(ε9643)

TABLE 2.—CALIBRATION RESULTS

Station	Shear, lb		Difference, percent	Bending, in-lb		Difference, percent	Torque, in-lb		Difference, percent
	Measured	Applied		Measured	Applied		Measured	Applied	
134	21,950	21,000	4.5	4,341,000	4,198,000	3.4	2,054,000	1,868,000	9.9
240	15,753	15,000	5.2	2,228,000	2,181,000	2.1	503,000	462,000	8.9
328	9,329	9,000	3.6	984,000	960,000	2.5	-235,000	-221,000	6.3

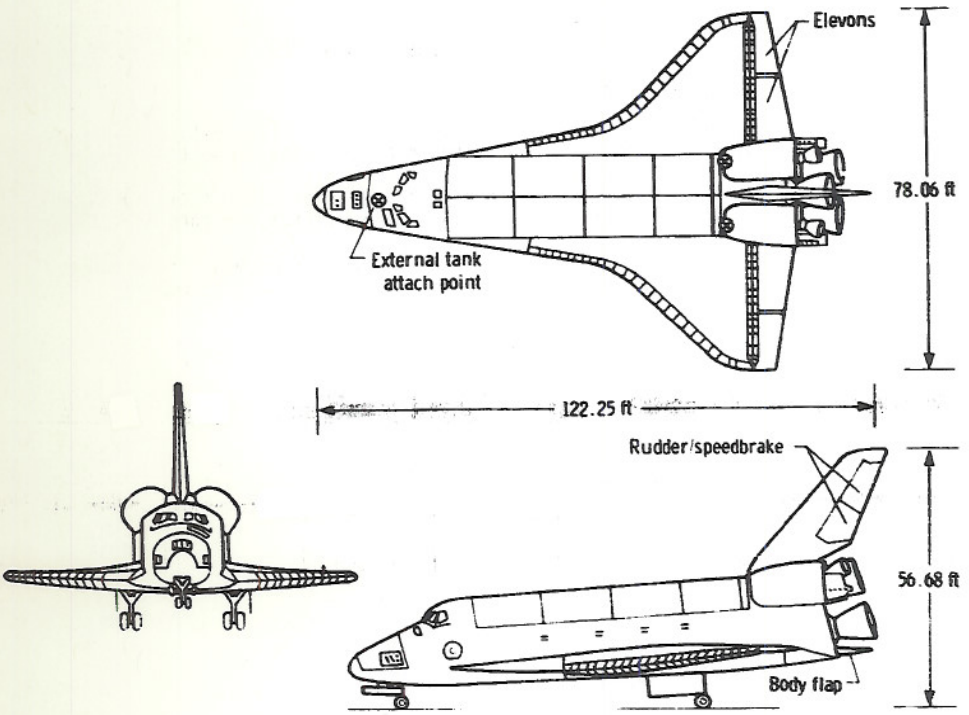

Figure 1. Orbiter configuration

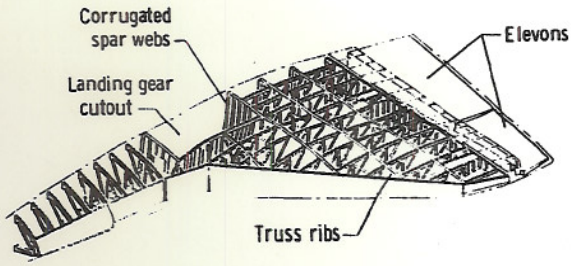

Figure 2. Orbiter internal wing structure

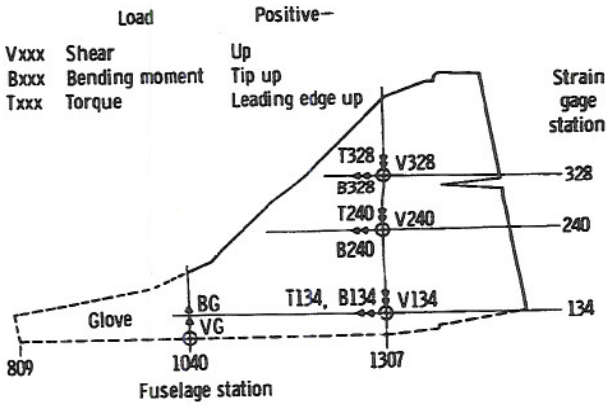

Figure 3. OV 102 wing load measurements

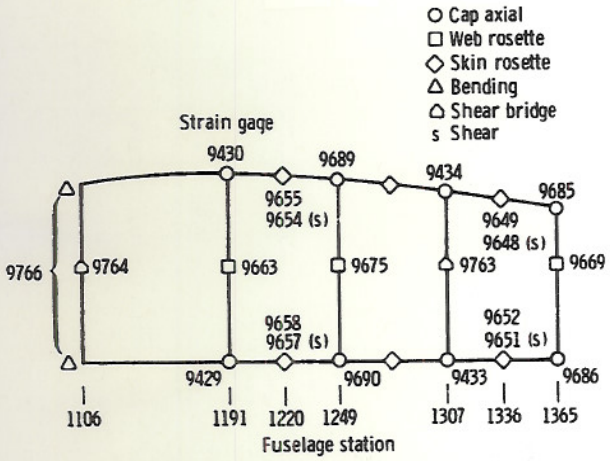

Figure 4. OV 102 wing strain gage locations for wing station 240

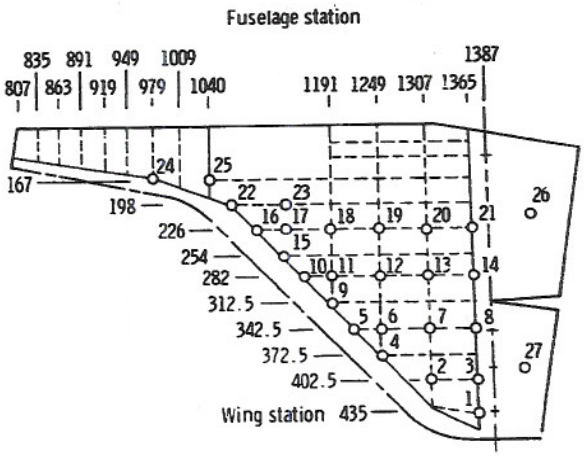

Figure 5. Right wing load points for calibration—10,000 pounds at each point serially (27 points)

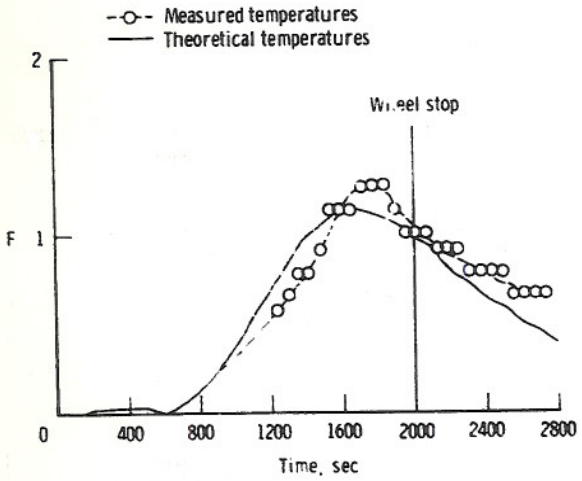

Figure 6. Thermal gradient ratio as a function of time

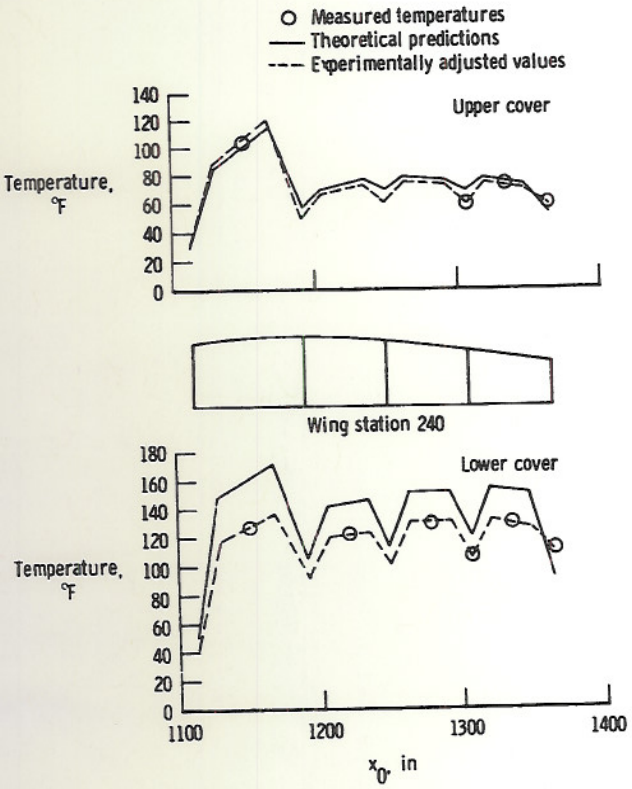

Figure 7. Temperature measurements at wing station 240

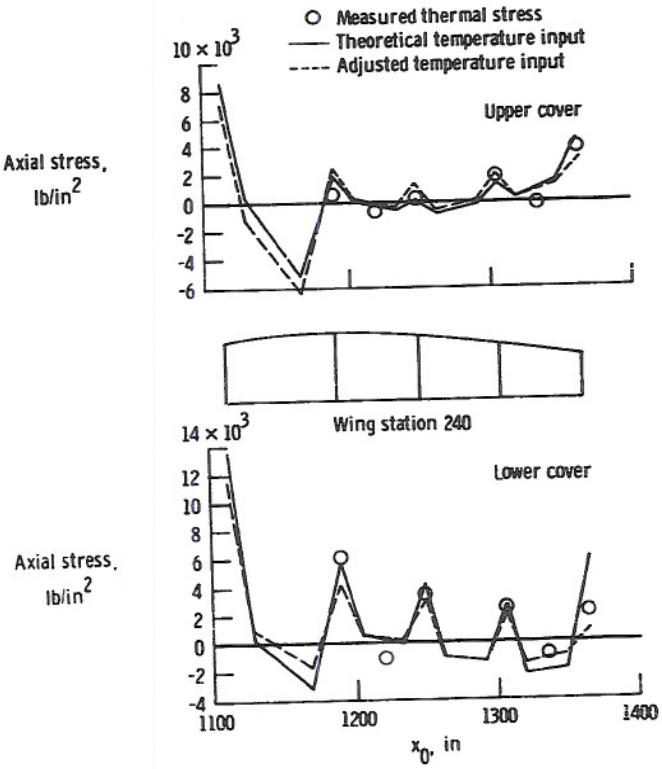

Figure 8. Thermal stress at wing station 240

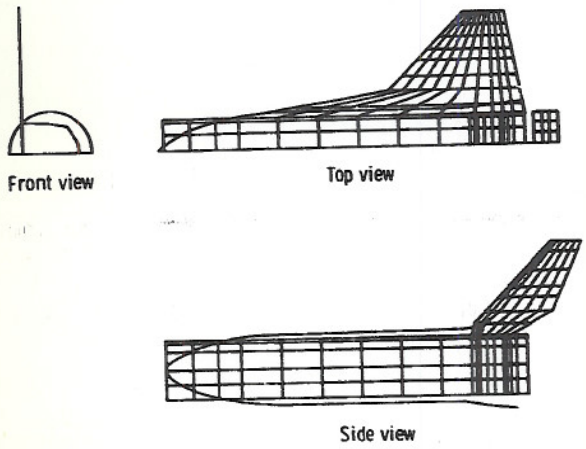

Figure 9. FLEXSTAB aerodynamic model

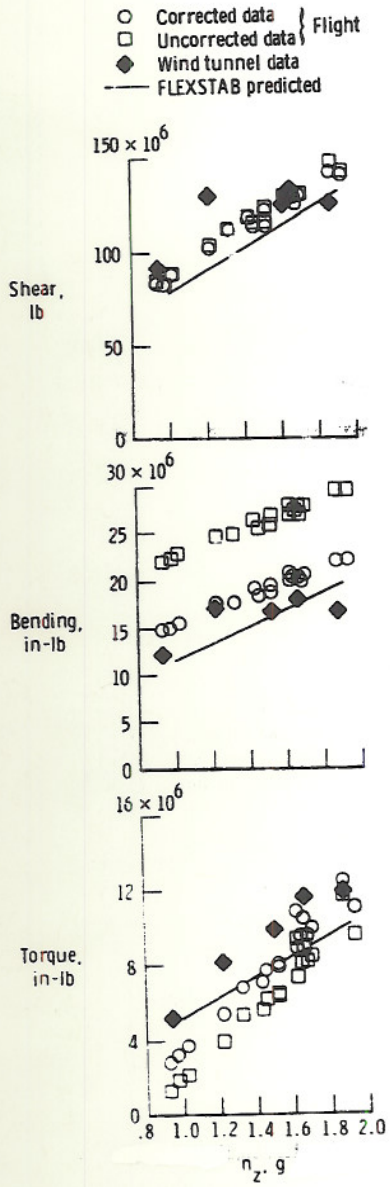

Figure 10. Loads at wing station 134, Mach 0.82 turn

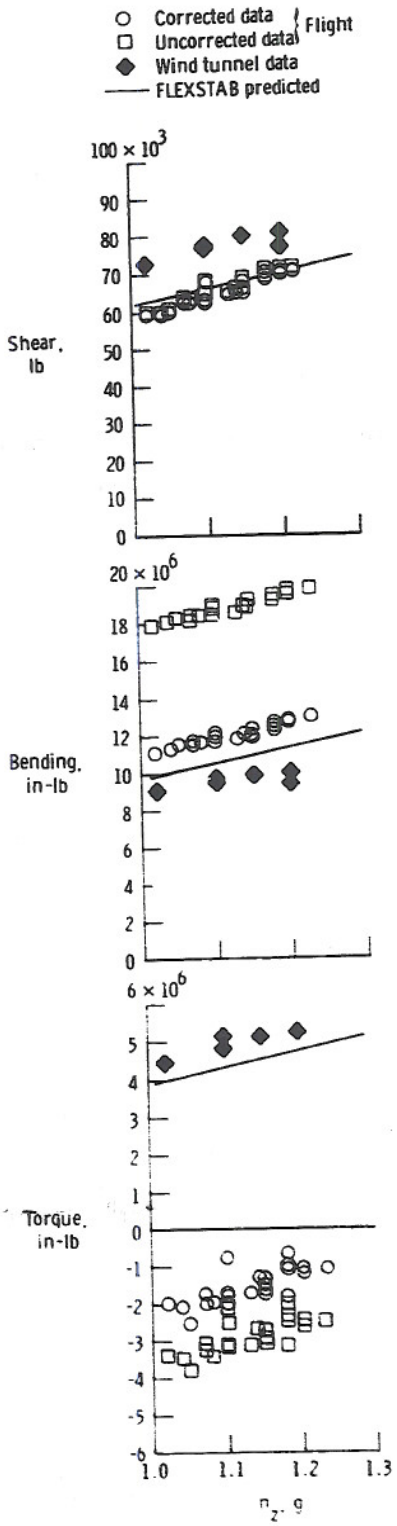

Figure 11. Loads at wing station 134, Mach 2.09 turn